2nd Micro and Nano Flows Conference
West London, UK, 1-2 September 2009

# Mathematical Modelling of Nanoparticle Delivery to Vascular Tumours

Rebecca J. SHIPLEY [1,2,*], Steven D. WEBB [3], Sarah L. WATERS [2], Steven R. McDOUGALL [4], Fiona ROBERTS [3]

* Corresponding author: Tel.: ++44 (0)1865 270744; Fax: ++44 (0)1865 202429;
Email: shipley@maths.ox.ac.uk
1: Christ Church, University of Oxford, UK
2: OCIAM, Mathematical Institute, University of Oxford, UK
3: Department of Mathematics, University of Strathclyde, UK
4: Institute of Petroleum Engineering, Heriott-Watt University, UK

**Abstract** The goal of any cancer therapy is to achieve efficient, tissue-specific targeting of drugs to cancer cells. However, most anticancer agents act on healthy and malignant tissue alike, potentially resulting in side effects to healthy tissue. This has motivated the development of treatment strategies that are cancer-cell specific; one approach uses biomimetic polymer vesicles (BPV) to deliver chemotherapeutic drugs into cells before releasing them. BPVs are synthetic membrane enclosed, nanometre-sized structures, and provide ideal drug delivery vectors because specific targeting to cancer cells can be achieved by coating with tumour-specific molecules.

We present several mathematical models covering a wide range of length-scales pertinent to BPV-mediated delivery protocols and focus on capturing the *in vivo* environment by evaluating the impact of the underlying vascular structure upon the governing transport mechanisms. Firstly, we present models of specific binding of BPVs to cancer cells. Subsequently we examine the implications of these model outputs in the contexts of both discrete capillary architectures and higher level homogenized-models that track blood and BPV transport at the tissue scale (both intra- and extra-tumorally). Numerical solutions are discussed, and recommendations are presented on that optimal integration of the models to generate quantitative predictions associated with BPV treatment efficacy.

**Keywords:** Biomimetic Polymer Vesicles, Cancer, Mathematical Modeling

## 1. Introduction

Biomimetic polymer vesicles (BPV) are membrane enclosed, nanometre-sized, structures composed of synthetic amphiphilic block copolymer (See Figure 1) [3]. BPV are self-assembled at neutral pH from synthesized amphilic copolymers that mimic the membrane forming ability of phospholipids [4]. They are similar to liposomes, which use naturally occurring lipids, but their wholly synthetic nature means that BPV can exhibit increased stability and reduced permeability [5,6]. Furthermore, vesicle stability is largely unaffected by surface coating with molecules, such as polyethyleneglycol (PEG), that improve the BPV 'stealth' properties and circulation time [3].

The purpose of this work is to use theoretical models to assess the feasibility of using BPVs to deliver chemotherapeutic drugs into cells before releasing them. Mathematical models will be used to address important questions relating to the infiltration of BPVs into tumours, their selective targeting of cancer cells and their mechanism of action once they reach the tumour.

The use of BPVs in cancer treatment has evolved from a previous treatment of targeting liposomes (containing anti-cancer drugs) to cancer cells. Liposomes are nanometer-sized vesicles that occur naturally in our cells, and have a lipid bilayer structure. These membranes are amphiphilic, and so contain a hydrophilic head and hydrophobic tail.

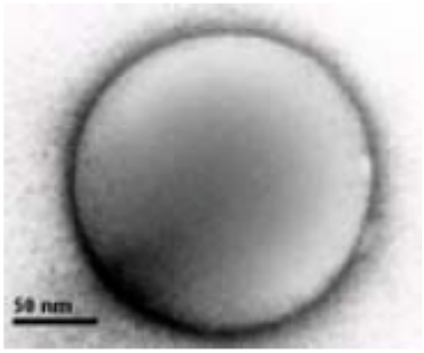


Figure 1: Biomimetic polymer vesicle which can encapsulate genes, drugs etc (picture courtesy of Giuseppe Battaglia, University of Sheffield).

Treatment using targeted liposomes was limited as they were leaky, could not be targeted efficiently and were quickly removed from the blood by the reticulondothelial system (immune system) [4]. BPVs on the other hand are completely synthetic, and so can be made with different properties by changing the composition of the polymers. Similar in structure to a liposome, BPVs are nanometer-sized spherical vesicles with an amphiphilic bilayer that self-assembles when the pH is raised (i.e. by adding water). During assembly drugs (such as chemotherapy agents) or DNA can be encapsulated.

The BPVs are assumed to be taken up by cells by receptor mediated endocytosis. This process involves receptors on the cell surface binding (reversibly) to specific ligands that are also located on the BPV surface. The cell membrane will then deform, creating a pit that allows more interactions between receptors and ligands. The membrane will encapsulate the BPV, and pinch off creating an organelle, an endosome. Due to the pH sensitive nature of the polymer, when the BPV is within the acidic endosome the vesicle will de-polymerize and release the payload (therapeutic drugs or DNA).

Treatment using BPVs has significant potential. However, there are still a number of outstanding questions: (1) what is the optimal number of ligands for BPV uptake? (2) what is the optimal diameter of the BPVs? (3) will unspecific uptake affect the quality of the treatment/surrounding cells? (4) how do BPV distribute through a tumour, and how should this impact BPV design? We address some of these issues in this paper.

## 2. BPV Binding Model

Firstly, we present a mathematical model of the binding of BPVs to cancer cells, via specific ligand/receptor interactions and endocytosis. The model is a system comprising of $n$+5 ODEs, where $n$ is the maximum number of (ligand:receptor) bonds that can be made between ligands on the BPV surface and receptors on the surface of the cell.

We let $V(t)$ be the total density of free BPVs per volume, and we define $L(t)=V(t)/l$, where $l$ is the (fixed) mol of ligands per BPV. The rate of change of $L(t)$ over time can be written as

$$\frac{dL}{dt} = -k_a LF + k_d \sum_{j=1}^{n} B^j,$$

where $k_a$ is the binding association rate constant and $k_d$ is the dissociation rate. The first term represents binding of BPVs to the cell (forming a single bound ligand:receptor complex), and the second is the total dissociation rate of bound complexes, where $B^j(t)$ represents the concentration of BPVs bound by $j$ ligand:receptor bonds. The rate equation for the concentration of single bound complexes is given by:

$$\frac{dB^1}{dt} = k_a LF - k_d B^1 - k_a\{\rho_l l N_A - 1\}\rho_f F B^1 - k_i B^1 + 2k_d B^2,$$

where the first term represents the initial binding of receptor to ligand and the second term is the dissociation rate of that bond. The third term represents the formation of a complex with 2 bonds, where $\rho_l$ and $\rho_f$ are the proportion of ligands and receptors on the BPV and cell, respectively, that are available for subsequent binding (this is determined by the tether length of the ligand and clustering rate of receptors etc.). The fourth term represents the internalization of the BPV (with an assumed constant rate $k_i$) and the fifth term arises from the dissociation of a

ligand:receptor complex from a double ligand:receptor bound BPV. Generalizing this expression for $i$ bonds, $B^i(t)$, yields

$$\frac{dB^i}{dt} = k_a\{\rho_l l N_A - (i-1)\}\rho_f F B^{i-1} - (ik_d + k_i)B^i - k_a\{\rho_l l N_A - i\}\rho_f F B^i + (i+1)k_d F B^{i+1}.$$

Here, $i=2,\ldots,n-1$, where $n$ is the maximum number of bonds that can form ($n \leq \rho_l N_A$). The equation for the concentration of BPVS bound by $n$ bonds, $B^n(t)$, is given by

$$\frac{dB^n}{dt} = k_a\{\rho_l l N_A - (n-1)\}\rho_f F B^{n-1} - (nk_d + k_i)B^n.$$

Associated with this binding, the concentration of free receptors per volume, $F(t)$, changes according to

$$\frac{dF}{dt} = -k_a\{LF + \sum_{j=1}^{n}(\rho_l l N_A - j)\rho_f F B^j\} + k_d\sum_{j=1}^{n} jB^j - d_f F + f(b_{tot})M,$$

| Parameter | Dimensional Value |
|---|---|
| $k_a$ | $3.7101\text{x}10^{8}$ cm$^3$mol$^{-1}$min$^{-1}$ |
| $k_d$ | $3.7101\text{x}10^{-5}$ min$^{-1}$ |
| $k_i$ | 0.05 min$^{-1}$ |
| $\rho_l$ | (0,1] |
| $\rho_f$ | (0,1] |
| $l$ | 1200 mol vesicle$^{-1}$ |
| $c_1$ | 0 min$^{-1}$cell$^{-1}$mol |
| $c_2$ | 0.03 min$^{-1}$cell$^{-1}$mol |
| $c_3$ | 0.5 mol cell$^{-1}$ |
| $d_f$ | 0.03 min$^{-1}$ |
| $\alpha$ | 1 |
| $\upsilon$ | $8.3\text{x}10^{-16}$ vesicle mol$^{-1}$ |
| $d_b$ | 0.01 min$^{-1}$ |
| $d_p$ | 1.2 min$^{-1}$ |
| $\beta$ | 1 |
| $N_A$ | $6.022\text{x}10^{23}$ mol$^{-1}$ |
| $\mu$ | 1.2 min$^{-1}$ |

Table 1 Parameter values

where,

$$f(b_{tot}) = c_1 + \frac{c_2 b_{tot}^{\alpha}}{c_3^{\alpha} + b_{tot}^{\alpha}} \quad \text{and} \quad b_{tot} = \tfrac{1}{M}\sum_{j=1}^{n} B^j.$$

The first term in the $F$-equation represents the loss of free receptors due to complex formation with BPV bound ligands, the second term denotes the freeing up of receptors after dissociation, the third term represents the natural half-life of receptors and the fourth term represents receptor production feedback which we assume is an increasing function of the total number of bound complexes.

The equation for internalized BPVs per volume, $B^{in}(t)$, is given by,

$$\frac{dB^{in}}{dt} = \frac{k_i}{l}\sum_{j=1}^{n} B^j - d_b B^{in},$$

The linear decay represented by the second term denotes the lysing of BPVs within an acidic endosomal vacuole. When the BPVs lyse, they then release their payload. In our case this is a therapeutic drug, $P(t)$. We thus have

$$\frac{dP}{dt} = \upsilon d_b B^{in} - d_p P.$$

Here, $\upsilon$ represents the concentration of drug encapsulated in each vesicle (mol/vesicle) and $d_p$ is the drug half-life.

Finally we have the equation for the tumour cell density, $M(t)$,

$$\frac{dM}{dt} = rM\left(1 - \frac{M}{K}\right) - g(\rho)M,$$

where we assume a logistic growth (with intrinsic proliferation rate $r$ and carrying capacity $K$), and a linear removal rate due to the BPV-drug treatment. We take

$$g(\rho) = d_m + \frac{\mu\rho^{\beta}}{P_0^{\beta} + \rho^{\beta}}, \text{ where } \rho = \frac{P}{M}.$$

We parameterize this model by using rate

constants associated with the analogous liposome treatment using folate receptor targeting (see, for example, [7]). Table 1 illustrates a base set of parameter values.

## 3. Analysis of the BPV Binding Model

In Figure 2, we show a typical numerical simulation of the ODE system described above. In this example, we take the maximum numbe of ligand:receptor bonds to be 20.

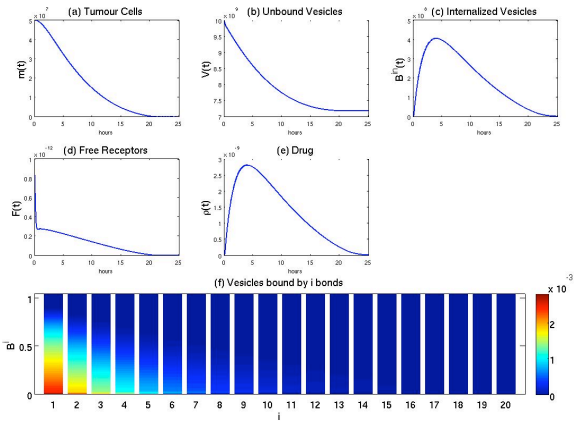


Figure 2 (a) – (e) shows tumour density, free BPVs, internalized BPVs, free receptors and drug per cell respectively over 24 hours. In (f), the $i^{th}$ bar represents vesicles bound by $i$ bonds. We take $\rho_l = \rho_f = 0.5$.

Over time, the free-BPVs bind to the available free-receptors on the cell surface, subsequent multiple binding then occurs (although, we notice that with this parameter set the BPVs are generally internalized rapidly after 4 binding events), the internalized BPVs then shed their drug load, within acidic endosomal vacuoles, which kills the tumour cells and the overall tumour density decreases.

Typically, we observe a fast transition in the free receptor solution as receptors are quickly bound by ligand on the infiltrating polymer vesicles. A singular perturbation analysis in the single binding case, with the number of ligands per vesicle being the large parameter controlling the perturbation, yields realistic approximation solutions and sheds insight into the solution behaviours during/and after this quick transition (details omitted for brevity).

We also examine the effect of receptor clustering and ligand tether length. We explore these effects by varying the parameters $\rho_f$ and $\rho_l$ between 0 and 1: 0 denoting the zero clustering case/short tether length and 1 denoting high receptor clustering/long tether length, for $\rho_f$ and $\rho_l$, respectively. Figure 3 shows an example of the simulation results.

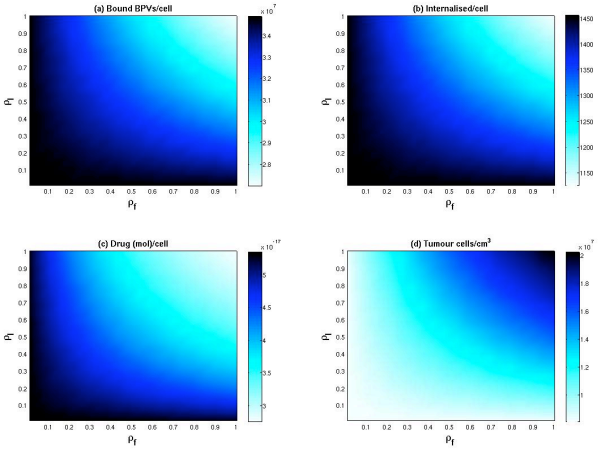


Figure 3 Effects of varying $\rho_l$, $\rho_f$ on (top left) bound BPVs/cell, (top right) internalized BPVs/cell, (bottom left) released drug concentration/cell and (bottom right) tumour cell density/cm$^3$.

An unexpected result from this parameter sensitivity analysis is that increasing receptor clustering and tether length (in effect, increasing the availability of 2-dimensional surface bonds) reduces the efficiency of the treatment. This result stems from the fact that, in our model, multiple binding events tend to delay BPV internalization and thus drug release. It is important to note, however, that the precise mechanisms of BPV internalization is largely unknown and other modes of endocytosis does exist, such as there being some optimal number of bonds for internalization and, as you'd expect these modes do indeed yield quantitatively differing results (not shown).

## 4. Implications of Vascular Architecture upon BVP Delivery.

Whilst it is clearly vitally important to examine the intricacies associated with BVP binding, there is also a need to understand the way in which these particles are transported in vivo. To this end, we have investigated a

number of issues associated with perfusion at the tissue scale (both intra- and extra-tumorally). We begin with a discussion of BVP transport within discrete capillaries feeding a solid tumour.

### 4.1 Discrete Vascular Growth

Flow modelling in a tumour-induced capillary network has been considered previously in papers by McDougall et al [10,11] and Stéphanou et al. [14,15]. In these papers, flow through vascular networks was modelled in order to investigate the efficiency of chemotherapy treatments as they passed from parent vessel to tumour surface via an associated capillary bed. The capillary bed was generated from an angiogenesis model proposed in [1] and vascular growth was described by a discrete formulation of the associated set of partial differential equations. This model has been adapted to consider BVP transport from 2 bounding parent vessels, with BVP concentration being monitored as blood flows both towards the tumour periphery and within the tumour mass itself.

Figure 4 shows the time evolution of BVP concentration following a 150 second bolus injection into two feeder vessels at concentration $C_{max}$ (BPVs enter from left to right). At each timestep, the total number of BVPs flowing into capillary junction (node) was calculated and BVP concentrations for all outflowing capillaries were updated via flow-weighted partitioning of the available BVP mass.

Tumour vasculature is intrinsically less well connected compared to that characterizing the peripheral capillary bed and is also extremely leaky. The snapshots in Figure 4 clearly show that perfusion rates are low at the tumour site and demonstrate how poor vessel connectivity within the tumour mass can lead to long residency times for any BPVs that reach the target. Subsequent BPV extravasation into the host tissue can also be monitored (Figure 5) and future work will focus upon coupling this tissue-scale model to BVP binding mechanisms and associated cell biology.

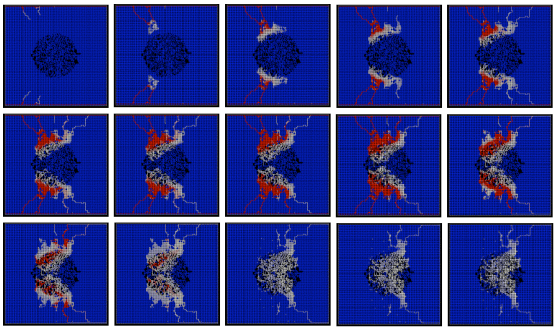

Figure 4: Simulated history of BPVs into vasculature surrounding centralized tumour: red = high BPV concentration, light blue = low BPV concentration.

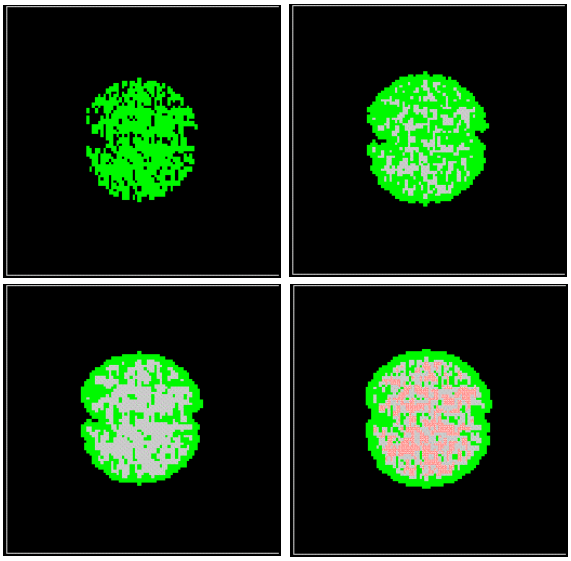

Figure 5: Transmural BPV transport from leaky tumour vasculature into tumour mass; pink = high extravasated concentration, green = low extravasated concentration.

### 4.2 Homogenization Approach

An alternative approach to predicting in vivo fluid and species perfusion is by simulating continuum models on the tissue-scale. These models must capture the vascular structure, and this may be achieved by using asymptotic homogenization to derive them. Homogenization has been applied to both fluid and species transport in vascular tumours [2.13]. Most pertinent to the modelling here is [13], where a model for fluid and drug transport through the leaky neo-vasculature and porous interstitium of a solid tumour is developed. The transport problems are posed on a micro-scale characterized by the inter-capillary distance, and the method of multiple scales is used to derive the continuum

equations describing fluid and drug transport on the length scale of the tumour. The fluid equations comprise a double porous medium, with coupled Darcy flow through the interstitium and vasculature, whereas the drug equations comprise advection-reaction equations; in each case the dependence of the transport coefficients on the vascular geometry is determined by solving micro-scale cell problems. The analysis is performed for a wide range of species transport properties, under the assumption of a periodic tumour microstructure.

The multiscale models of [13] are extended to capture the hierarchical vascular structure of dorsal skinfold chambers in [14]. Dorsal skinfold chambers are observation chambers that are implanted into an animal for intravital microscopy of the living tissue, and are widely used to test new anticancer agents before they reach the clinic. Once the tumour xenograft is transferred to the chamber, a fine catheter is inserted into the jugular vein and the carotid artery, passed subcutaneously to the dorsal side of the neck, closed, and stitched to the chamber frame. Angiogenesis occurs to vascularize the tissue from the seeded vein and artery; the resulting microvasculature is categorized in terms of arterioles, capillaries and venules. The arterioles and venules are larger than the capillaries, and connect directly to the seeded artery or vein, respectively; the capillary bed connects the arterioles to the venules, and hosts transfer of agents to the tumour interstitium. Example data on the arteriole, capillary and venule diameters, and the intercapillary distance for nude mice and hamsters are presented in Table 2.

| Measurement (μm) | Nude Mice [9] | Hamsters [8] |
|---|---|---|
| Arteriole Diameter | 37.4 ± 12.8 | 42.2 ± 14.1 |
| Capillary Diameter | 5.6 ± 1.8 | 6.1 ± 1.4 |
| Venule Diameter | 41.5 ± 10.6 | 46.5 ± 13.0 |
| Intercapillary Distance | 37 ± 15 | 54 ± 28 |

Table 2: Arteriole, capillary and venule diameters, and intercapillary distances in dorsal skinfold chambers in nude mice and hamsters.

The final fluid transport equations of [14] comprise a quadruple porous medium with coupled Darcy flow through the arterioles, venules, capillary bed and interstitium. The drug transport equations comprise coupled advection-reaction equations for the total species concentration in each of the four domains. Here we apply precisely the same models to predict the perfusion of BPVs in a dorsal skinfold chamber. We investigate two delivery protocols: delivery by a single injection, and delivery by constant perfusion.

In each case, we solve the chamber-scale models of [14] using the finite elements package 'COMSOL Multiphysics' on the 2D domain shown by Figure 4. The chamber is represented by a unit square with a central circle of malignant tissue; a source artery and sink vein are seeded in the same position, to one edge of the malignant tissue. A key ingredient of the models we use is that the explicit dependence of the transport coefficients on the vascular geometry is known. We assume that the arterioles and venules have the same regular structure, but test four different vascular structures for the capillaries. The four different vascular structures are shown in Figures 5-8. The first, Figure 5, represents a grid network, whilst Figure 6 takes a hexagonal structure. This hexagonal structure is also used for the arterioles and venules, and the capillaries in the healthy tissue. Figures 7-8 represent two more irregular (and arbitrary) networks that may be more realistic to malignant capillary morphology; we refer to them as 'irregular-I' and 'irregular-II' respectively.

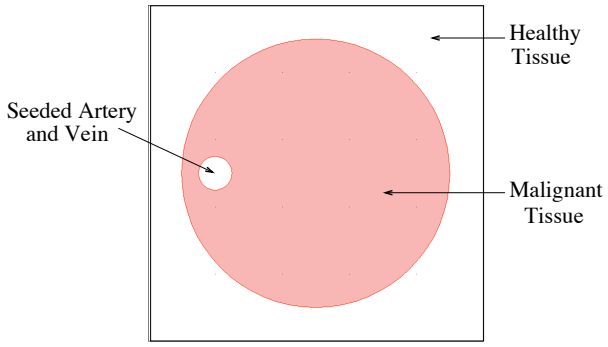


Figure 6: The chamber structure as drawn in COMSOL. The chamber is a square with a central circle of malignant tissue, surrounded by healthy tissue. A source artery and sink vein are seeded in the malignant section.

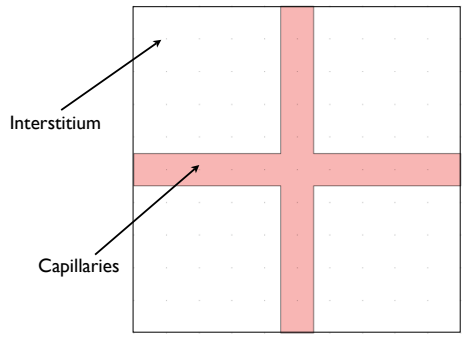


Figure 7: The periodic grid vascular structure.

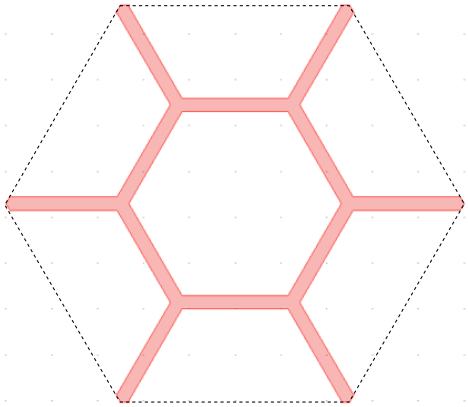

Figure 8: The periodic hexagonal vascular structure.

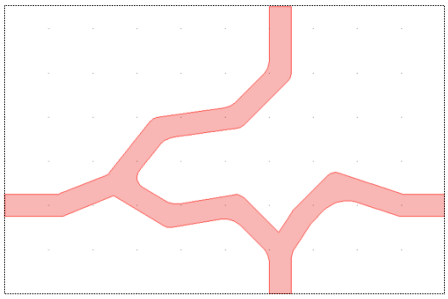

Figure 9: The periodic 'irregular-I' vascular structure

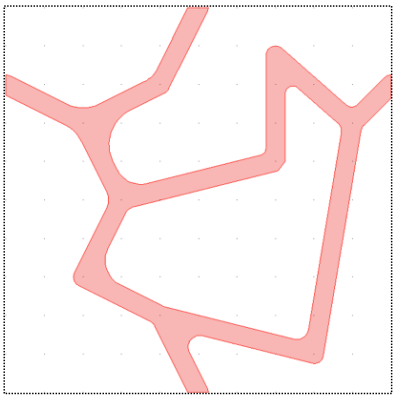

Figure 10: The periodic 'irregular-2' vascular structure

### 4.2.1 Single Injection

For an injection, we test an initial dose of BPV of ≈2700 nM. This dose will be metabolized in the bloodstream as time progresses. We follow the protocol for vinblastine (an anticancer drug), which assumes that this metabolism occurs over four phases [12]; an initial fast phase that represents the distribution of the blood through the body, and three further slow phases representing the redistribution and metabolism of the drug in different organs of the body. This can be represented mathematically by the function

$$\sigma(t) = Ae^{-k_1 t} + Be^{-k_2 t} + Ce^{-k_3 t} + De^{-k_4 t},$$

where $k_1$=41.6 min$^{-1}$, $k_2$=0.17 min$^{-1}$, $k_3$=1.3×10$^{-2}$ min$^{-1}$ and $k_4$=5.9×10$^{-4}$ min$^{-1}$ represent the half lives of the four separate phases, and A, B, C, D are constants determined for a specific individual (we use A=1557nM, B=862nM, C=261nM and D=20nM). The function σ(t) is used as a boundary condition on the total arteriole BPV concentration on the seeded artery wall.

The total BPV concentration in the arterioles, venules, capillary bed and interstitium in the malignant tissue is given by

$$\hat{c}_i^{\text{tot}} = \frac{1}{\text{Volume of Malignant Domain}} \int_{\text{Malignant Domain}} \hat{c}_i \, \mathrm{d}V.$$

The total concentration of BPVs in the interstitium is pertinent to assessing BPV delivery; this is presented as a function of time, and for a single injection, in Figure 11.

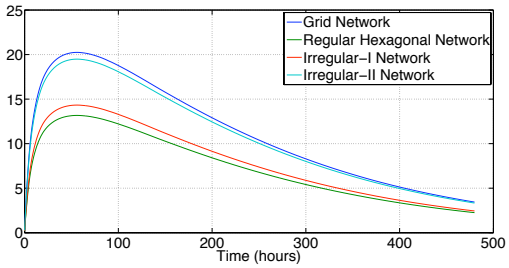


Figure 11: Total BPV concentration in the interstitium, as a function of time, and for a single injection (nM).

### 4.2.2 Constant Perfusion

For constant perfusion of BPVs, a constant concentration of BPVs will be maintained in the bloodstream for a longer period of time. We consider an indicative value of 8nM

applied constantly over a period of 5 days, and apply the boundary condition

$$\sigma(t) = \begin{cases} 8\text{nM} & \text{for } 0 \le t \le 120 \text{ hours} \\ 0 & \text{for } t > 120 \text{ hours} \end{cases}$$

The total BPV concentration in the interstitium is plotted as a function of time, and for constant perfusion, in Figure 12.

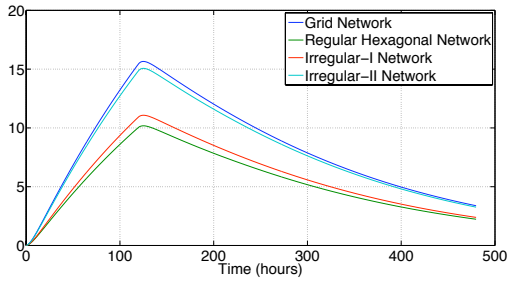


Figure 12: Total BPV concentration in the interstitium as a function of time for constant perfusion (nM).

This modelling approach provides a mechanism for quantitatively predicting BPV delivery to cancerous tissue for a range of delivery protocols and underlying vascular structures. Future work will focus on integrating this approach with the discrete modelling approach of Section 4.1, together with BVP binding mechanisms and associated cell biology.

## 5 Conclusions and Extensions

In this paper we have developed models pertinent to BPV-mediated delivery protocols over a range of length-scales. Firstly, we presented a model that describes binding of BPVs to cancer cells, via ligand/receptor interactions and endocytosis. Next we investigated the dependence of BPV-delivery to tissue on the underlying vascular structure and delivery mechanism.

Future work will focus on integrating the models presented here, and developing them further. Firstly, the discrete and homogenized approaches will be used for mutual validation (this is essential to form concrete predictions of blood and BPV perfusion properties). Next, they will be extended to explicitly capture the outputs of the BPV-binding models. BPV-transport will also be coupled to models for $H^+$, oxygen and chemotherapeutic agent transport. In this way, we will develop a rigorously validated *in vivo* model for BPV-mediated delivery of anti-cancer agents that may be used to optimize the treatment protocol.

## References

[1] Anderson, A. and Chaplain, M., 1998. Bull Math Biol **60**: 857-900.
[2] Chapman, S.J., Shipley, R.J. and Jawad, R., 2008. Bull Math Biol **70**(8): 2334-2357.
[3] Discher, D.E. and Ahmed, F., 2006. Ann. Rev. Biomed **8**:323-341.
[4] Discher, D.E. and Eisenberg, A., 2002. Science **297**(5583): 967-973.
[5] Battaglia, G. and Ryan, A.J., 2005. J. Am. Chem. Soc. **127**(24):8757-8764.
[6] Discher, B.M., Won, Y.-Y., Ege, D.S., Lee, J.C.-M., Bates, F.S., and Discher, D.E., 1999. Science **284**(5417):1143-1146.
[7] Ghaghada, K.B., Saul, J., Natarajan, J.V., Bellamkonda, R.V., Annapragada, A.V., 2005. J. Controlled Release **104**:113-128.
[8] Lehr, H., Guhlmass, A., Nolte, D., Keppler, D., Presta, M., Denekamp, J., 1991. J Clin Invest **87**:2036-2041.
[9] Lehr, H., Leunig, M., Menger, M., Nolte, D., Messmer, K., 1993. American Journal of Pathology **143**(4): 1055-1062.
[10] McDougall, S.R., Anderson, A.R.A., Chaplain, M.A.J., Sherratt, J.A., 2002. Bull Math Biol **64**(4): 673-702.
[11] McDougall, S.R., Anderson, A.R.A., Chaplain, M.A.J., 2006. Journal of Theoretical Biology **241**(3): 564-589.
[12] Owellen, R. Hartke, C., Hains, F., 1977. Cancer Research **37**:2597-2602.
[12] Shipley, R.J. and Chapman, S.J., 2009. *Multiscale Modelling of Fluid and Drug Transport in Vascular Tumours*. Submitted.
[13] Shipley, R.J., Chapman, S.J. and Roose, R., 2009. *A Theoretical Investigation of Fluid and Vinblastine Transport in Dorsal Skinfold Chambers*. In preparation.
[14] Stéphanou, A., McDougall, S.R., Anderson, A.R.A., and Chaplain, M.A.J., 2005. Math Comp Mod **41**(10): 1137-1156.
[15] Stéphanou, A. McDougall, S.R., Anderson, A.R.A. and Chaplain, M.A.J., 2006. Math Comp Mod **44**:96-123.